Articles

Planning Dosimetry Near Vascular Ports

New research shows the effects of electron beams on implanted vascular access ports composed of plastic, determining how they impair the fluence of radiation around them.

view

4-D Tools and Radiation Treatment Planning

One of the most important recent advances in radiation oncology has been the integration of 4-D treatment planning tools into the clinic. 4-D treatment tools have enabled the radiation oncologist...

view

OIS: Efficiency and Accessibility Are Key Factors

Radiation oncologists and most clinicians involved in the field prefer to spend their time treating patients, not sitting in front of a computer. Yet today more than ever, they are being tasked...

view

NEW TECHNOLOGY

Hitachi to Distribute iCAD's MRI Image Analysis, Guided Biopsy Software

iCAD's SpectraLook with PrecisionPoint image

Imaging Technology NEWS

Planning Dosimetry Near Vascular Ports

New research shows the effects of electron beams on implanted vascular access ports composed of plastic, determining how they impair the fluence of radiation around them

By: Michael S. Gossman, M.S., DABR and David Coll-Segarra, M.S.

October 6, 2011

Figure 1: Bard Access Systems vascular access ports, starting at left, are: low-profile titanium model 0605490, Rosenblatt model 0654970, MRI Powerport model 1808000, ultra low-profile model 0655640, X-Port duo port model 0607650, low-profile MRI port model 0603880 and plastic hard base model 0604520.

Since their first appearance in medicine in 1969, subcutaneous vascular access ports have been used regularly by healthcare providers to provide chemotherapy and antibiotics and to monitor blood chemistry without having to tap into veins continuously.*[1,2,3]* A vascular access port is most simply described as a hollow reservoir with a silicone septum on top, which is attached to a small catheter. The penetrable septum allows for the direct access of a needle for injection or collection of fluids through the reservoir.

Since these devices are in such common use, they often are being used in patients referred for radiation therapy. In such instances, radiation oncologists often find it difficult when the device is in the way of a targeted tumor. For this reason, it is scientifically important for medical physicists to examine how foreign materials implanted in the body affect radiation treatment dosimetry.

Researchers have investigated consequences of attenuation and scatter through various metals and involving high-density prosthetics. Research in one group showed that back-scattering from bone-titanium interfaces of mandibular implants can be appreciated to nearly -14% in a 6 MV X-ray beam.*[4]* Bridging plates contain more metal than vascular access ports do. However, this prior study provided early evidence that therapy beam dose distributions should be considered, as some vascular access ports are now constructed with such metals.

Previous Studies Identify Attenuation Levels

The first study of the dosimetric effects of X-rays and electron beams for vascular access ports was conducted by Bagne et al in 1990.*[5]* The ports available at that time were made mostly of titanium or steel. Using a variety of radiation detectors, his group showed there is a sizeable decrease in dose if the port is located directly in the path of the beam. A significant discovery of -51.5% attenuation was announced for one port in a 9 MeV electron beam. X-ray attenuation was determined to be -17% at 6 MV and -14.5% at 10 MV for stainless steel devices.

In 1994, Noriega et al used film to continue this work and plotted the off-axis profile of X-ray beams when metal ports were imbedded in a phantom. For photons only, attenuation was found to be -17.5% for 6 MV and -10% for 15 MV.6 For each of these efforts, attenuation was found to decrease with increasing energy.*[5,6]*

Since then, technology has improved, and a new generation of ports containing plastic is now available. In 2006, a research team published an extensive study of the 15 different classifications of vascular access ports for their affect in an X-ray beam.*[3]* The research detailed changes in dose distributions as recognized by pencil-beam and convolution superposition algorithms in comparison to Monte Carlo simulations.

For locations beyond the device, the maximum change in dose was found to be as much as -16.8% in attenuation for 6 MV photons and -7.2% for 18 MV photons. Dose increases of 7% for back-scatter and side-scatter locations were discovered for a titanium port. It has only recently been suggested that electron beam attenuation through nonmetal ports may be clinically feasible.*[7]*

New Research Evaluates Plastic Ports

The scope of this new study was to characterize the dosimetric effect on external beam electron radiation when directed upon plastic vascular access ports. The study also determines whether there is a difference between similar port designs affecting radiation treatment regimens, and if port placement alternatives or radiation therapy should be avoided.*[8,9,10]* This research integrated a variety of seven representative models from Bard Access Systems, a company which encompasses approximately 30% of all vascular access ports used in medicine in the United States. *[3,11]*

The ports used in this work were made primarily of plastic, except for one made of titanium. Noteworthy specimens included the MRI Powerport and the Rosenblatt port. The Rosenblatt model had a little metal on the base and existed with a dual lumen design. The MRI Powerport is made of radiotranslucent material, so it is specially designed not to interfere with imaging techniques. This research incorporated devices of diverse design and varying dimension (see Figure 1).

The experimental phantom setup included a 420 cm3 miniature water phantom made of polystyrene. This phantom was placed on top of a Sun Nuclear MapCheck 1175 silicon diode array. Natural water at 1.5 cm depth was added to completely submerge each vascular access port under investigation. The MapCheck diode array was centered in the electron beam using mounted room lasers, an optical distance indicator light field projection cross-hair and bubble level. In order to simulate the saline solution that pulmonologists use to flush all air from the inside cavity of the vascular access port, water was injected identically for all devices.

Attenuated absorbed dose results were acquired using a MapCheck diode array with version 5.0 software. The electrometer software was capable of cumulative charge collection for up to 445 diodes during irradiation. It also was proficient to profile results across any two-dimensional plane. This setup was incorporated for attenuation measurements at electron energies of 9-20 MeV.

We wanted the detectors to be at a depth ideal for measurement at the energy chosen. Given that the silicone diodes in the MapCheck device are inherently sealed in 2 cm plastic, this depth was determined inappropriate for 6 MeV electron beams, as it was near to the practical range. Consequently, the attenuation exhibited in a 6 MeV beam required the use of a Kodak EDR-2 ReadyPak film instead of the MapCheck device.

To measure lateral scatter, a PTW TN31014 ionization chamber with sensitive volume 0.015 cm3 was connected to a Capintec 192 electrometer. The chamber was placed 1 cm from the port and affixed with an adhesive to the bottom of the container. No build-up cap was needed, since the thimble was entirely submerged.

To measure back-scatter with a port in place, the chamber was directly positioned on top of the port, immediately above the dense rim. A build-up cap was then used, where a portion of the thimble protruded anterior to the water surface. The distance from the ionization chamber to the point of measurement was 0.3 cm, as determined by the build-up cap thickness and thimble radius (see Figure 2).

The particle accelerator was a Varian 21EX, programmed to deliver electron beams with energies of 6, 9, 12, 16 and 20 MeV. Machine calibration was achieved for each electron beam to produce 1 cGy/MU at the depth of maximum dose in a 10 x 10 cm2 field. A 100 cm source-to-surface distance defined by the center of rotation of the accelerator was maintained for all measurements.

A larger 20 x 20 cm2 open field cone was selected for use with all experiments, since it was observed in prior studies to have ideal properties of flatness and symmetry. This aperture defined the electron beam collimation for all measurements. Attenuation, lateral scatter and back-scatter were each determined for all seven vascular access ports by comparing results with and without them being in the path of the beam. Measurements were averaged over multiple runs at 100 monitor units and with radiation being delivered at a dose rate of 600 cGy/min.

Dose Profiling

From diode array dose profiling data saved and analyzed at 9-20 MeV electron beam energies, the comparison of diode readings with the port in place to those when the port was removed provided the beam blocking effect magnitude. The maximum changes in absorbed dose were qualitatively evaluated by overlaying each profile on the same plot. The numerical percentage variation was computed given the spreadsheet values at each diode location.

Numerical tabulated data for the 6 MeV electron beam were characteristic of the dose response to the ReadyPak film. Each calibration film and test film was developed using an AFP ImageWorks Mini-Medical 90 processor and analyzed using an X-Rite 301 point densitometer. A Hurter & Driffield calibration curve was generated by relating the optical density of the same batch of film observed at different dose levels. Dose profile attenuation plots were fashioned similarly by scaling these results along a graduated path.

Scatter measurements were conducted identically for all vascular access ports investigated. Although dose profile plots were not made possible in the lateral and backward direction, various readings were achieved around each device to ensure the result represented the location of maximum scatter effect.

The equation found at the end of this article provides the calculation used for all attenuation and scatter measurements.

Discussing the Findings and Implications

Dose profile plots that were generated had discernible uniqueness. A flat and symmetric plot was measured when the vascular access port was not positioned in the phantom. For measurements conducted when the device was immersed, considerable dose reduction was made readily apparent in many cases. Dose reduction caused by attenuation altered the topographical profile in the immediate vicinity of the location of the device. Figure 3 provides the 6 MeV profile for the low-profile titanium port, which shows the maximum of all effects caused by attenuation in this research.

Close inspection of the floor of the profile when the port was inserted suggests construction of the device in that plane is markedly identical. A review of technical data provided from the manufacturer supports this finding. Simple inspection of the dose profile indicates the magnitude of changes observed across the field.

Symmetry is also observed at the elevated edge of the profile as it began to flatten out. According to the known radius of the low-profile titanium port at 1.24 cm (length 2.48 cm) in comparison to the scaled dose change illustrated, ranging outward from 1.2-1.8 cm, this dose region exists beyond its material construction. It is then

conclusive that the dose variation observed at this location is a direct result of bremsstrahlung radiation being created, as the incident electron beam interacts with the material.

This recoil radiation is not purely lateral. Rather, it is forward scattered at an oblique angle. Figure 4 illustrates the direction of X-ray scatter from a high-energy electron beam when incident upon dense media.*[11,12]*

The enhanced dose level above the 100% line indicates that incident fluence of radiation downward is predominantly unchanged and that dose was measured at those locations to signify additional fluence redirected there when the electrons interacted with the port rim. As hypothesized, the densest material used in the design of this port created the largest change at the lowest electron energy. At higher electron energies, less attenuation and scatter were seen in line-dose profiles. Figure 5 provides an example of absorbed dose reduction measured after the beam passed through a port model composed of plastic.

Like the low-profile titanium port, the Rosenblatt port also causes symmetric dose distributions with respect to attenuation. Given the known radius of the Rosenblatt port at 1 cm (length 2.01 cm), symmetry was not observed for forward, obliquely directed out-scattering. However, the significance of a slightly greater amount of out-scattering is consistent with the polar plot showing greater amounts of bremsstrahlung radiation for less dense media. These data indicate a clear example that a dual-lumen vascular access port, such as that of the Rosenblatt model, can have a distinctly different effect on the incident radiation beam.

The results of all measurements are presented in Table 1. In general, the greatest variation in lateral scatter is for lower energies, 6 and 9 MeV. A more bulky port design seems to have a greater impact on changes in scattering than the material of the device. Back-scatter does not seem to be very significant, with higher values around only 1%.

The Rosenblatt port showed dose attenuation at -49% for 6 MeV. At higher energies of nominally 16 to 20 MeV, the device caused less attenuation at -16% comparatively. The remainder of ports was made of plastic. Registered dose change effects for each of these were documented. The MRI Powerport and the X-port Duo, both of considerable size, showed maximum attenuations of about -16% for 6 MeV. All other ports showed maximum absorbed dose variance of less than -10% at all electron energies.

An increase in absorbed dose in the adjacent environment of the port was observed mostly in ports with metal parts at high energies (16 and 20 MeV). The greatest attenuation was presented by the low-profile titanium port, with dose reductions by as much as -62% for 6 MeV electrons. At 9 MeV, attenuation for this port was -32% degradation in transmitted fluence.

Although the ports studied by Bagne et al were different, this result is considerably different than the -51.5% change seen by that group at 9 MeV.5 Still, the finding supports the need to correctly identify the energy and port model when correlating the overall effects provided here, in assistance with clinical applications.

Conclusions

To recap our findings: Although higher energy electron beams were shown to penetrate these dense devices with less attenuation, as much as -16 to -21% dose changes were identified by some models. Still, negligible attenuation was observed for some plastic ports at all therapeutic energies.

Results indicate that lateral scatter from a vascular access port for electron beams can alter expected dose by as much as 2.9%, while expected dose in the back-scatter direction can change by a maximum of 1.2%. Since metal port results show changes far greater than effects exhibited by plastic ports, it is conclusive that any port with a mix of plastic and metal should be treated with greater caution when calculating dose.

The levels of dose change should be specifically cautioned to the radiation oncologist as they consider treatment through these devices. This research proved that some electron beams may have sufficient ability to penetrate vascular access ports for therapeutic purposes when the density is nonmetallic.

Although as much as -60% attenuation was measured for one specific port tested, not all port models exhibited the same effect. Substantially less dose variations were concluded for plastic ports. Higher-energy electron beams were

distorted the least, in general. Each result is dependent on the specific model of port being used and the electron beam energy of interest.

Therapeutic medical physicists should be aware of the impact metal and plastic vascular access ports have on high-energy electron beams. When identified as a clinical barrier, consultation with the implanting physician should be sought, where options for port relocation or removal can be considered.

Some port models have a material composition and design that appears to cooperate with the interest of the physician to pass radiation directly through them toward their target structure. We suggest these results be used to assist medical physicists in assessing the feasibility of passing therapeutic electron radiation through a vascular access port to target a structure anatomically posterior to it.

Michael S. Gossman, M.S., DABR, is chief medical physicist and RSO, Tri-State Regional Cancer Center, radiation oncology department, Ashland, Ky. David Coll-Segarra, M.S., is employed by CNMC Co. Inc. (c/o Best Medical International Inc.), located in Nashville, Tenn. *This research was supported by a Bard Access Systems Grant #7019 issued to Gossman. It was presented at the American Association of Physicists in Medicine - Ohio River Valley Chapter Spring Symposium in Cincinnati, Ohio, in March 2011.*

References:

1 Broviac JW, Cole JJ, Scribner BH. "A silicone rubber atrial catheter for prolonged parenteral alimentation." Surg Gynecol Obstet. 1973; 136(4):602–06.
2 Dillon PA, Foglia RP. "Complications Associated With an Implantable Vascular Access Device." Journal of Pediatric Surgery. 2006; 41:1582-1587.
3 Gossman MS, Seuntjens JP, et al. "Dosimetric effects near implanted vascular access ports: an examination of external photon beam dose calculations." J Appl Clin Med Phys 2009; 10(3):3-15.
4 Mian TA, Van Putten MC Jr, Kramer DC, et al. "Back-scatter radiation at bone-titanium interface from high-energy X and gamma rays." Int J Radiat Oncol Biol Phys. 1987; 13(12):1943–47.
5 Bagne FR, Merrick HW 3rd, Samsami N, and Dobelbower RR Jr. "Radiation dose perturbation in the presence of permanent vascular-access injection ports." Int J Rad Oncol Biol Phys. 1990; 18(2):463–67.
6 Noriega BK, Feygelman V, Sanders RM. "Radiation attenuation characteristics of venous access devices. Navan." 1994; 1:12–14.
7 Coll-Segarra D. "Dosimetric effects near implanted vascular access ports under external electron beam radiation." Wright State University Masters Degree Thesis, Dayton, Ohio, 2010.
8 Lehmkuhl L, Denecke T, Warschewske G, et al. "Multislice computed tomographic angiography for pre-interventional planning of port placement for intra-arterial hepatic infusion chemotherapy." J Comput Assist Tomogr. 2007; 31(1):66–71.
9 Gullane PJ. "Primary mandibular reconstruction: analysis of 64 cases and evaluation of interface radiation dosimetry on bridging plates." Laryngoscope. 1991; 101(6 Pt2 Suppl 54):1–24.
10 Hudson FR, Crawley MT, Samarasakera M. "Radiotherapy treatment planning for patients fitted with prostheses." Br J Radiol. 1984; 57(679):603–08.
11 IMS Health. "Medical Device Market Report, Q2 2007." Plymouth Meeting Executive Campus, Plymouth Meeting, Pa., USA.
12 Schiff LI. "Energy-angle distribution of betatron target radiation." Phys Rev. 1946; 70:87.
13 Johns HE and Cunningham JR. "The Physics of Radiology (4th Ed.)." Charles C. Thomas Publishing, Springfield, Ill., 1983, pp. 67.

FIGURE 2

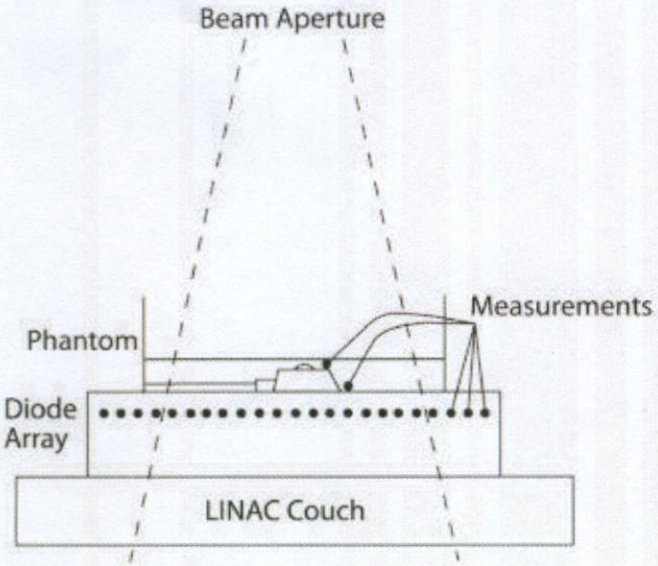
Beam Aperture
Measurements
Phantom
Diode
Array
LINAC Couch

FIGURE 3

6 MeV Profile: Low Profile Titanium Port

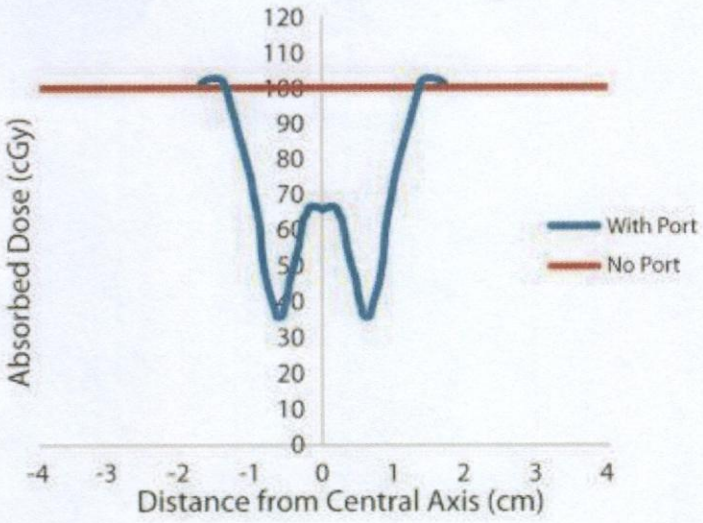

FIGURE 4

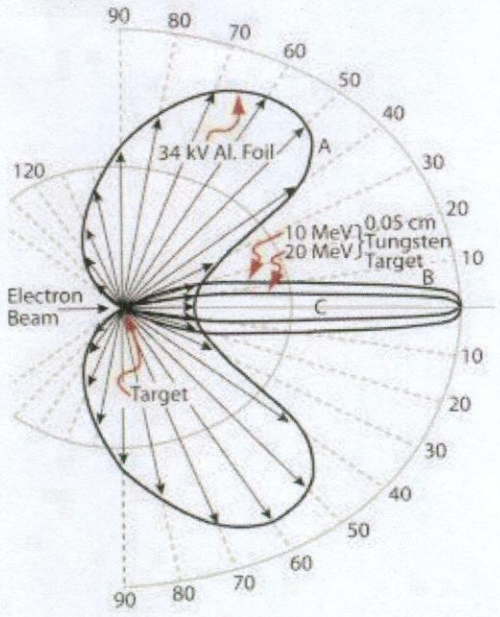
90
80
70
60
50
40
30
20
10
120
34 kV Al. Foil
A
10 MeV
20 MeV
0.05 cm
Tungsten
Target
B
C
Electron
Beam
Target
10
20
30
40
50
60
70
80
90

FIGURE 5

20 MeV Profile: Rosenblatt Port

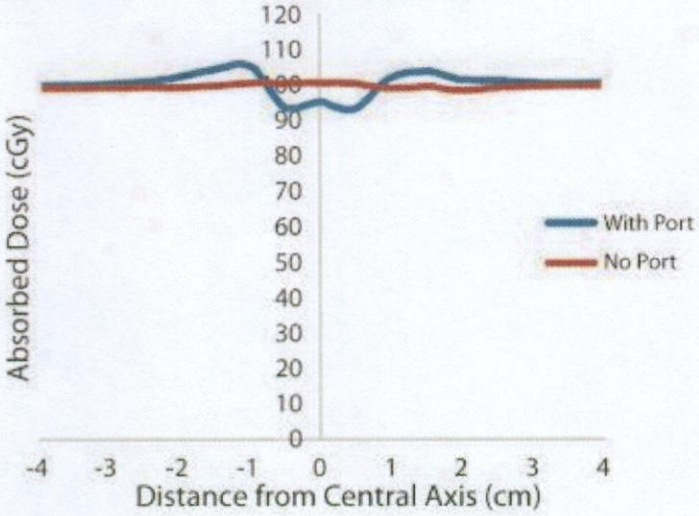

Table 1.

(a) 6 MeV

Port	*Attenuation*	*Lateral Scatter*	*Back-scatter*
LOW PROFILE TITANIUM	-64.3 %	0.0 %	0.0 %
ROSENBLATT	-49.9 %	0.6 %	0.0 %
MRI POWERPORT	-19.1 %	1.8 %	1.0 %
ULTRA LOW PROFILE	-5.8 %	1.3 %	0.0 %
X-PORT DUO	-14.8 %	1.3 %	1.0 %
LOW PROFILE MRI	-5.6 %	0.9 %	0.0 %
PLASTIC HARD BASE PORT	-6.8 %	1.3 %	0.3 %

(b) 9 MeV

Port	*Attenuation*	*Lateral Scatter*	*Back-scatter*
LOW PROFILE TITANIUM	-32.2 %	2.4 %	0.5 %
ROSENBLATT	-23.0 %	1.4 %	0.5 %
MRI POWERPORT	-15.1 %	2.9 %	1.0 %
ULTRA LOW PROFILE	-9.1 %	1.9 %	0.5 %
X-PORT DUO	-9.1 %	1.9 %	0.5 %
LOW PROFILE MRI	-5.1 %	1.4 %	0.8 %
PLASTIC HARD BASE PORT	-8.9 %	1.9 %	1.0 %

(c) 12 MeV

Port	*Attenuation*	*Lateral Scatter*	*Back-scatter*
LOW PROFILE TITANIUM	-27.3 %	1.9 %	0.0 %
ROSENBLATT	-20.5 %	0.9 %	0.2 %
MRI POWERPORT	-8.5 %	1.4 %	1.2 %
ULTRA LOW PROFILE	-4.3 %	0.9 %	0.2 %
X-PORT DUO	-5.1 %	0.9 %	0.5 %
LOW PROFILE MRI	-2.0 %	0.5 %	0.2 %
PLASTIC HARD BASE PORT	-3.9 %	0.9 %	0.7 %

(d) 16 MeV

Port	*Attenuation*	*Lateral Scatter*	*Back-scatter*
LOW PROFILE TITANIUM	-20.2 %	1.3 %	0.0 %
ROSENBLATT	-15.7 %	0.4 %	0.0 %
MRI POWERPORT	-5.0 %	1.1 %	0.9 %
ULTRA LOW PROFILE	-2.8 %	0.8 %	0.2 %
X-PORT DUO	-3.5 %	0.7 %	0.5 %
LOW PROFILE MRI	-1.6 %	0.4 %	0.5 %
PLASTIC HARD BASE PORT	-2.6 %	0.7 %	0.7 %

(e) 20 MeV

Port	*Attenuation*	*Lateral Scatter*	*Back-scatter*
LOW PROFILE TITANIUM	-21.6 %	0.0 %	0.0 %
ROSENBLATT	-15.8 %	0.0 %	0.0 %
MRI POWERPORT	-3.7 %	0.2 %	0.9 %
ULTRA LOW PROFILE	-1.4 %	0.4 %	0.4 %
X-PORT DUO	-3.2 %	0.2 %	0.7 %
LOW PROFILE MRI	-0.9 %	0.2 %	0.4 %
PLASTIC HARD BASE PORT	-2.5 %	0.2 %	0.9 %

$$dD = 100\% \left[\frac{D_{Nafion} - D_{Pore}}{D_{Nafion}} \right]$$